Submitted to Journal of the European Ceramics Society on 23th July 2019/ Revised 18th Oct/ Accepted 29th Oct.

# Medium infrared transparency of MgO-$MgAl_2O_4$ directionally solidified eutectics

Bibi Malmal Moshtaghioun [a*], Jose I. Peña [a], Rosa I. Merino [a]

[a]Instituto de Ciencia de Materiales de Aragón, CSIC-Universidad de Zaragoza, 50018 Zaragoza, Spain

## Abstract

$MgAl_2O_4$-MgO eutectic ceramics have been fabricated by the laser floating zone method. Increasing growth rates from 10 to 50 mm/h, the microstructure transformed from irregular MgO rod-to-lamellae phase and it approached to almost homogeneous rod morphology. At the highest used velocity of 750 mm/h, the cell structure was completely dominant and the samples were free from transversal cracks. Although the highest flexure strength was found at 750 mm/h growth rate, the maximum optical transmittance in the medium-infrared range was obtained for 50 mm/h growth rate and for 1mm thick samples reached values higher than 75% in the wavelengths between 4 and 5.3µm.The enhanced transmittance for the sample with 50 mm/h growth rate can be explained in terms of the close refraction indexes of the component phases and the characteristic lengths of the resulting microstructure showing fully dense ceramics with the finest and almost homogeneous microstructure.

*Keywords*: $MgAl_2O_4$-MgO eutectic; Laser floating zone; MIR transparent ceramics

* Corresponding author: Bibi Malmal Moshtaghioun; mali@unizar.es, mali_moshtagh@us.es

doi published manuscript: 10.1016/j.jeurceramsoc.2019.10.053 (Available online: 2 Nov 2019)

## 1. Introduction

Ceramics composed of several phases are studied in the frame of many different applications. Frequently it is for structural purposes (better mechanical properties), but this comes usually combined with other functional properties rendered to the material by the appropriate properties combination of the components, as thermal or electrical conductivity, optical activity, electronic or magnetic properties, etc. In particular, examples of ceramics for optical applications in which it is required or take advantage of multiple phases or gradient in composition are light guiding materials[1], hosts for selective doping or multiple active ions in lasers [2,3], phosphors or scintillators [4], selective emitters with low emissivity in the IR [5,6], or metamaterials [7-9] etc .An approach- for creating multiphase composites, exhibiting useful microstructure/texture patterns, is the directional solidification of eutectics (DSE)[10,11]. One of the techniques most used -for DSE work, especially in the case of systems from which transparency may be expected- is the laser floating zone (LFZ) method [10 ,11]. LFZ is an excellent method among the different directional solidification procedures to grow ceramic oxides from the melt, as the large thermal gradients at the liquid/solid interface achieved with this method allow high growth rates to be used. Actually, a $CO_2$ laser is focused on the molten zone and a precursor is brought into the focused laser beam. Growth starts by moving the precursor and mass conservation dictates that the diameter can be reduced as the square route of the feed rate-pull rate ratio. Moreover, the control of the crystal microstructure is possible by means of growth rates. Let us note that the LFZ can generate pores free parts- a feature critical in the case of transparent ceramics [10, 11].

One of the systems, that may be of interest for DSE processing (LFZ variant), is the spinel-MgO eutectic. From both components monolithic bulk parts of high transparency were

already obtained by powder- sintering [12-25]. They are high melting point materials, have relatively large thermal conductivity [26] with transparency window extending deep into the IR (5.3 μm for $MgAl_2O_4$ and 6.8 μm for MgO) [27].In both cases, fully dense ceramics can only be fabricated at high sintering temperatures coupled with high pressure. Therefore, high isostatic pressure (HIP) and spark plasma sintering (SPS) are the most efficient techniques, so far [12-25].

Advances in the manufacture of both materials have been made, and results can be found in the literature [15,19,20,25], optimizing powder characteristics with impurity level to ppm range and particle size of less than 100 nm, rigorous compaction and sintering schemes by HIP and/or SPS to obtain fully dense ceramics with nanograin retention, or post annealing treatment to avoid color-center formation. Therefore, large pieces of thickness in the mm range with in-line transmittance up to 80 % in the visible range can be obtained.

Some preliminary studies- regarding the fabrication, by LFZ, of bulk pieces, from the spinel-MgO eutectic- have been already effectuated. It was observed that specimens strength is larger when high pulling rates are used[28- 32];the studies also showed that solidification , at pull rates lower than 50 mm/h causes - owing mostly to the thermal expansion mismatch of the two phases- cracking, thus severely reducing strength[29,30,32].

Further work is needed in order to fully master the LFZ fabrication of parts,from the spinel-MgO eutectic. In this context, the purpose of this workis to study the relative in-line transmittance of the MgO-$MgAl_2O_4$ eutectic ceramics, which were solidified by LFZ and the effects of variable growth rates on the in-line transmittance and microstructure of the MgO-$MgAl_2O_4$ eutectic ceramics were investigated and correlated.

## 2. Experimental procedure

The starting materials were commercially available $Al_2O_3$powder (Sigma-Aldrich, 99.99%) and MgO powder (Sigma-Aldrich,>99%). MgO powder was dried in a furnaceat 1200 ºC for 12 h to remove the possible moisture absorption from outside air [33].The eutectic point of MgO and $MgAl_2O_4$appears at 55wt% $Al_2O_3$ and 45 wt% MgO and its melting temperature is around 2000 ºC [34]. Two general approaches using lasermelting techniques were studied for the possible fabrication of this eutectic ceramic with dense and fine microstructure retention.

The first was solidification of the eutectic rods by directional solidification from the melt using the laser-heated floating zone (LFZ) method with a $CO_2$ laser [10]. Precursor rods of ~ 3 mm in diameter and up to 5 cm in length were prepared by cold isostatic pressing for 5 min at 200 MPa followed by pre-sintering in a furnace at 1500 ºC for 12 h. The pre-sintered rods were then grown by LFZ in air, in all cases using two steps of diameter reduction at a pulling rate of 300 mm/h. These two first steps were performed in counter-rotation of the crystal and precursor with 50 rpm which provided fully dense rods grown from the melt without residual porosity. The last (third)step, however, was performed without rotation and the solidified rod being pulled downwards using growth rates between10 and 750 mm/h to evaluate its effect on the microstructure, average grain size, relative in-line transmittanceand strength of the resulting $MgAl_2O_4$-MgO eutectic ceramics. A nominal laser output power of 40-50W has been used in the last step to maintain a constant feed and very small molten zone and the temperature of the melt was estimated as 2200 ºC by digital laser pyrometer. Eutectic rods of ~1 mm were fabricated.

Later on, the transverse cross-sections of the grown eutectic rods and plates were first cut, ground and polished to a 0.25 μm finish. Additionally, all were characterized microstructurally by a field emission scanning microscopy(FE-SEM)(model Merlin, Carl Zeiss, Germany) with an

EDS microanalysis system INCA350 from Oxford Instruments or a SEM (model 6400, JEOL, Tokyo, Japan). Microstructure observations were done from both transverse and longitudinal sections using the back-scattered emission (BE) mode on carbon coated-polished surfaces.

In-line transmission spectra were measured in the VIS-NIR range with a Cary 5000 UV-Vis-NIR spectrometer from Agilent and in the MIR range with a Spectrum 100 FTIR spectrophotometer form Perkin-Elmer. The instruments overlap in the 2.5 to 3.0 microns wavelength range, but the transmittance was not coincident on all samples, most probably due to different optical arrangement and apertures. Therefore, the short-wavelength (VIS-NIR) spectra were scaled to match the measurements in the MIR range. Calculation of transmission spectra of Mie-scattering [35] of spheres was made using Scott Prahl´s software [36].

Finally the strength of rods in longitudinal direction for the highest grown velocity was measured by flexural tests carried out in a three-point bending test fixture with 10 mm loading span in Instron testing machine (Instron 5565). Eight tests were performed at constant crossheads speed of 0.05 mm/min.

## 3. Results and discussion

Directional solidification by the laser assisted floating zone method (LFZ) is frequently performed counter-rotating feed rod and pulling crystal as this better homogenizes the heating flux around the melt. Often, this also adds instabilities in the melt that lead to the formation of bands associated to the rotation period, that is, periodic changes in the microstructural size of the eutectic preferential solidification of one of the phases of the eutectic. Perturbation of the microstructure in composites leads to perturbation in the diffusion of light in the material.

Therefore we have solidified the samples without rotation and compared when necessary with the composite solidified with counter-rotation [29].

### *3.1. Microstructure of LFZ processed eutectic $MgAl_2O_4$-MgO*

Fig. 1 compares representative transverse cross section images of the $MgAl_2O_4$-MgO eutectic ceramics grown at different velocities without rotation. In Table 1 the microstructural properties obtained from the analysis of the SEM images are summarized.By EDS analysis, the bright matrix was detected to be spinel and dark embedded phases were MgO. It is worth knowing that transverse cracks were present for those samples solidified at a pulling rate lower than 100mm/h. In the areas with coarser microstructure, microcracks tend to appear, which lead to poor mechanical resistance [29]. At the lowest growth rates of 10 and 25 mm/h, the microstructure consisted of irregular MgO rod-to-lamellae phase in a continuous $MgAl_2O_4$ matrix (Figs. 1(A) and (B)). The transverse size of MgO phase was estimated from <width+length>/2 and are around 4.3 μm (Fig. 1(A), inset) and 3.2 μm (Fig. 1 (B), inset), respectively. Increasing the growth rate to 50 mm/h, a mixed microstructure was observed that indicates transition from rod-to-lamellae to rod morphology (Fig. 1(C)). At this velocity,MgO rods with triangular section with size of 0.8 μm(Fig. 1(C), inset)and rod-to-lamellae MgO structure with size of 1.9 μm was distinguished. Approaching 100 mm/h growth rate, therod-to-lamellae microstructure was almost transformed and the solidification suffered a transition to the formation of cells especially in the center (core of 380 μm diameter) of the solidified ceramic (Fig. 1(D)) which was surrounded by MgO fibrous microstructure in the approximately 250 μm thick outer shell of the sample. At this velocity, cells with a diameter of ~35μm and a boundary of ~13 μm in thickness were found. MgO fiber size was estimated about 0.9 μm(Fig. 1(D), inset)

and 7.1 μm inside and in the boundaries of the cells. While in the outer shell, the equivalent diameter of MgO fibers reached to 2.25 μm. The volume fractions for these three microstructure categories can be estimated to 32, 32 and 36 %, respectively. At the highest used velocity of 750 mm/h, the cell structure was completely dominant with a cell diameter about 27 μm and a boundary of ~7 μm in thickness(Fig. 1(E)). MgO fibers were found to size0.34 μm and 2.1 μm and with almost the same volume fraction inside and in the boundaries of the cells, respectively (Fig. 1E, inset). In the core (center) region of the samples solidified at 750 mm/h, two more features appear. A third bright phase was observed at the cell boundaries in the sample solidified at this rate (Fig. 1(E)). EDS microanalysis showed it contains O, Ca, Al, Si and Mg, suggesting it is consequence of the segregation of impurities towards the melt upon solidification. Occasionally some dendrites of MgO were observed, too.

### *3.2. In-line transmittance*

MgO and $MgAl_2O_4$ are transparent materials, with a common transparency window from 360 nm to 5400 nm. Their refractive index of the pure compounds [37-39] is not much different from one another. The ratio $nMgO/nMgAl_2O_4$ lies between 1.011 and 1.028 in this wavelength range, and therefore fully dense composites mixing both materials are expected to show small scattering and with the appropriate microstructure could show even transparency. Except for microcracking, the above given microstructures (Table 1) consist of approximately 25 % volume MgO phase disperse into the $MgAl_2O_4$ matrix, with transverse dimension of the MgO particles between 0.4 and 7 microns. Along the pulling direction the dispersed phase will show elongated shape, as corresponds to the directional solidification process.

Figure 2 shows the in-line transmittance of 1 mm thick transverse slices of the composite solidified without rotating feed- and grown-rods in order to avoid excessive coarsening of the microstructure. All the samples show some degree of transparency in the medium infrared (MIR), which is larger in the sample solidified at 50 mm/h. Slower or faster pulling rates result in smaller in-line transmittance. At wavelengths larger than 5.5 μm absorption by phonon excitation in the component materials takes place, and the transmittance decreases. At low wavelengths, extinction is due scattering by the material microstructure.

Maximum in-line transmission occurs along the solidification direction and when perturbation of the solidification process is avoided. This can be seen in Figs.2 (upper curves) and 3. Figure 2 (upper curves) shows the measured transmittance of two pieces solidified at 50 mm/h. The dotted-line curve corresponds to a sample that was mounted with better parallelism of the solidification direction and in-line transmission axis, together with a smaller diaphragm so that the central region of the sample is explored with the measuring light beam. Misalignment of the sample upon cutting the transverse cross section or due to curvature of the solid-liquid interphase causes the measured transmission to decrease (continuous versus dotted orange curvesin Fig. 2). Figure 3 shows in-line transmission curves of transverse and longitudinally cut slices with counter-rotation. That is, in-line transmission is measured along the solidification direction or perpendicular to it, respectively. It is evident that across the solidification direction the samples show smaller in-line transmittance at both pulling rates.

The fact that the samples solidified at 50 mm/h show the largest transmittance can be rationalized taking into account the microstructure of the samples. Low pulling rates (10 mm/h to 50 mm/h) tend to show coupled growth with homogenous microstructures with smaller microstructural features as pulling rate increases. At 50 mm/h pulling rate the microstructure

shows signs of departure from coupled growth and incipient cell formation, but still not well developed. An average transverse particle size can be used to describe the transverse size of the MgO dispersed phase (see Table 1). At even larger pulling rates, the formation of cells is evident in part (100 mm/h) or all the sample cross-section (750 mm/h). This leads to transverse size of the MgO particles which is finer inside the cells and coarser in the inter-cell areas. Light scattering is expected to be smaller when the microstructure is finer and more homogeneous, and this happens in the samples solidified at 50 mm/h, mostly when banding is avoided.

We have not attempted to calculate the theoretical transmittance in this material, which at minimum would require modelling the anisotropic sample microstructure in a way that is simultaneously representative of the samples microstructure and tractable computationally. Instead, to serve as a guide for the analysis of in-line transmittance results, we have performed a simple calculation consisting of the calculation of scattering cross-section of spheres of MgO embedded in $MgAl_2O_4$. Each component material is characterized by its refractive index given in references 37, 38 and 39. The sphere diameters used in the calculations are the equivalent diameter of the MgO particles sizes taken from relevant transverse cross-section SEM micrographs. When the sample microstructural features have clearly distinguishable populations, a volume percentage and equivalent size was assigned to each microstructure. To estimate an extinction coefficient, the number of particles per unit volume was calculated using this filling ratio of MgO, that was taken as f = 0.245 [29]. The volume fraction is large enough so that multiple scattering and particle interaction could be contributing to the scattering. We did not take this into account. Although the density of particles is large, we expect trends in this simpler calculation to mimic the trends in the overall behavior of the material transmission. The reason is that the refractive index contrast is small, so that the scattering strength is also small in the NIR.

For example, at$\lambda$= 4.5 μm, the predicted extinction length for 2 μm diameter spheres is 1.6 mm (corresponding to particle extinction efficiency 0.00335 with 0.0585 particles per $\mu m^3$).

Figure 4 shows the result of the calculations. Reflection at the surfaces of the slices has also been taken into account. Transmission is moderate with MgO spheres of 4.3 μm diameter (black curve), and increases as the diameter of the MgO particle decreases (red, brown and orange curves). The simulation to the 100 mm/h sample calculates the transmittance as a weighted average of the transmittance estimated for different sized spheres, as suggested by the microstructure. Therefore, although the microstructural size inside the cells is smaller, the transmittance decreases because of the populations with larger microstructural features, as is also observed experimentally. Overall, the microstructural sizes of the sample solidified at 750 mm/h is smaller, and thus the calculated transmittance increases again, contrary to what is observed experimentally. Most probably, the presence of other phases at the inter-cell areas should be blamed for the discrepancy. Segregation of impurities can be avoided with starting products with higher purity but the occasional formation of MgO dendrites is growth instability of much uncertain avoidance.

### *3.3. Flexural strength*

Three-point bending tests were just performed forthe grown rods with the rate of 750 mm/h which were free from transverse cracks to go into their flexural strength behaviour. No plasticity was observed. A strength value of ~445 MPa was obtained. This is around twofold greater than those (150-200 MPa) of conventional $MgAl_2O_4$ceramics [13,14] and nearer to the values reported for fine-grained SPS´ed Spinel [40]. Furthermore, mild improvement of strength was found compared with its counterpart grown with counter-rotation under identical

LFZconditions (i.e., 345 MPa) [29], which is because better homogeneity of microstructure by minimizing possible instabilities in the melt produced by periodic perturbations.

## 4. Conclusions

MgO-$MgAl_2O_4$eutectic ceramics show light transmission in the MIR. The transmittance arises because the fabrication procedure attains fully dense composite material, with small refractive index contrast between the component phases. In-line transmittance is maximum when the material is solidified at 50 mm/h. Transverse slices 1mm thick have values at or above 75 % at wavelengths between 4 and 5.3 μm. These are the solidification conditions that attain at the same time the finest and still rather homogenous microstructure in the material. Transmission is larger along the solidification direction, corresponding to the aligned microstructure.

Regarding mechanical properties, LFZ rods of around 1mm in diameter and solidified at 750 mm/h without using counter-rotation of the feedstock and growing crystal found to be the optimal condition to get highest flexure strength. This value amounts to 445 MPa and presents slightly better flexure strength than its counterpart solidified with counter-rotation. The formation of cracks at low solidification rates could not be avoided.

**Acknowledgements.** This work was supported by the Ministerio de Economía y Competitividad (Government of Spain) and FEDER Funds under Grants No. MAT77769-R, and Gobierno de Aragon (Grupo Reconocido DGA T02_17R) and the associated EU Regional Development Funds.BMM wants to acknowledge the support of the Spanish MINECO by means of a “Juan de la Cierva-Incorporación” fellowship during her sabbatical stay in Zaragoza.Authors

would like to acknowledge the use of the Servicio General de Apoyo a la Investigación- SAI, Universidad de Zaragoza, namely, the Service of the Electronic Microscopy of Materials.

## References

1. N. Yasui, Y. Ohashi, T. Kobayashi, T. Den, Development of Phase-Separated Scintillators with Light-Guiding Properties, Adv. Mater. 24 (2012) 5464.
2. R. I. Merino, J. A. Pardo, J. I. Peña, V. M. Orera, Microstructure-size dependence of the 1.520 μm Er+3 luminescence lifetime in $Al_2O_3$-$ZrO_2$ eutectic melt growth composites, App. Phys. Lett. 80 (2002) 589.
3. R. Balda, S. García-Revilla, J. Fernández, R. I. Merino, J. I. Peña, V. M. Orera, Near infrared to visible upconversion of Er3+ in $CaZrO_3$/CaSZ eutectic crystals with ordered lamellar microstructure, J. Luminescence, 129 (2009) 1422.
4. Y. Ohashi, N. Yasui, Y. Yokota, A. Yoshikawa, T. Den, Submicron-diameter phase-separated scintillator fibers for high-resolution X-ray imaging. App. Phys. Lett., 102 (2013) 051907.
5. N. Nakagawa, H. Ohtsubo, Y. Waku, H. Yugami, Thermal emission properties of $Al_2O_3$/$Er_3Al_5O_{12}$ eutectic ceramics. J Eur Ceram Soc, 25 (2005) 1285.
6. M. C. Mesa, P. B. Oliete, R. I. Merino, V. M. Orera, Optical absorption and selective thermal emission in directionally solidified $Al_2O_3$-$Er_3Al_5O_{12}$ and $Al_2O_3$-$Er_3Al_5O_{12}$-$ZrO_2$ eutectics, J. Eur. Ceram. Soc., 33 (2013) 2587.
7. R. I. Merino, M. F. Acosta, V. M. Orera, New Polaritonic Materials in the THz Range made of Directionally Solidified Halide Eutectics. J. Eur. Ceram. Soc., 34 (2014) 2061.
8. D. A. Pawlak, Metamaterials and photonic crystals –potential applications for self-organized eutectic micro- and nanostructgures. Scientia Plena 4 (2008) 014801.

9. M. Kafesaki, A. A. Basharin, E. N. Economou, C. M. Soukoulis, THz metamaterials made of phonon-polariton materials. Photonics Nanostructures: Fundam. Appl., 12 (2014) 376-386.
10. J. LLorca, V.M. Orera, Directionally solidified eutectic ceramic oxide, Prog. Mater. Sci. 51 (2006) 711.
11. R. I. Merino, J. I. Peña, A. Larrea, G. F. de la Fuente, V. M. Orera, Melt grown composite ceramics obtained by directional solidification: structural and functional applications, Recent Res. Devel. Mat. Sci. 4 (2003) 1.
12. A. F. Dericioglu, A. R. Boccaccini, I. Dlouhy, Y. Kagawa, Effect of chemical composition on the optical properties and fracture toughness of transparent magnesium aluminate spinel ceramics, Mater. Trans., 46 (2005) 996.
13. A. Goldstein, A. Goldenberg, M. Vulfson, Development of a technology for the obtainment of fine grain size, transparent $MgAl_2O_4$ spinel parts, J. Ceram. Sci. Tech., 2(2011)1.
14. O. Tokariev, T. Van Gestel, M. Bram, J. Malzbender, Strength enhancement of transparent spinel ceramics, Mater. Lett. 107 (2013) 364.
15. A. Krell, J. Klimke, T. Hutzler, Advanced spinel and sub-µm Al2O3 for transparent armour applications, J. Eur. Ceram .Soc. 29 (2009) 275.
16. A. Goldestein, A. Goldenberg, M. Hefetz, Transparent polycrystalline $MgAl_2O_4$ spinel with submicron grains, by low temperature sintering, J. Ceram Soc. Jpn. 117 (2009)1281.
17. K. Morita, B.N. Kim, K. Hiraga, H. Yoshida, Fabrication of transparent $MgAl_2O_4$ spinel polycrystal by spark plasma sintering processing, Scripta Mater. 58 (2008) 1114.
18. G. Bonnefont, G. Fantozzi, S. Trombert, L. Bonneau, Fine grained transparent $MgAl_2O_4$ spinel obtained by spark plasma sintering of commercially available nanopowders, Ceram. Int. 38 (2012) 131.

19. M. Sokol, M. Halabi, S. Kalabukhov, N. Frage, Nano-structured $MgAl_2O_4$ spinel consolidated by high pressure spark plasma sintering (HPSPS), J. Eur. Ceram. Soc. 37 (2017) 755.
20. A. Zegadi, M. Kolli, M. Hamidouche, G. Fantozzi, Transparent $MgAl_2O_4$ spinel fabricated by spark plasma sintering from commercial powders, Ceram. Int. 44 (2018) 18828.
21. K. Itatani, T. Tsujimoto, A. Kishimoto, Thermal and optical properties of transparent magnesium oxide ceramics fabricated by post hot-isostatic pressing, J. Eur. Ceram. Soc. 26 (2006) 639.
22. R. Chaim, Z. Shen, M. Nygren, Transparent nanocrystalline MgO by rapid and low temperature spark plasma sintering, J. Mater. Res. 19 (2004) 2527.
23. T. B. Tran, S. Hayun, A. Navrotsky, R. H. R. Castro, Transparent nanocrystalline pure and Ca-doped MgO by spark plasma sintering of anhydrous nanoparticles, J. Am. Ceram Soc. 95 (2012) 1185.
24. S. Wakahara, T.Yanagida, Y. Fujimoto, V. Chani, M. Sugiyama, Y. Futami, A. Yoshikawa, Phosphorescent luminescence of pure magnesium oxide transparent ceramics produced by spark plasma sintering, Opt. Mater. 35 (2013) 558.
25. X. Chen, Y. Wu, Fabrication and optical properties of highly transparent MgO ceramics by spark plasma sintering, Scripta Mater. 162 (2019) 14.
26. B. Schulz and M. Hoffmann, Thermophysical properties of the system $Al_2O_3$-MgO, High Temp.- High Pres. 34 (2002) 203.
27. W.J. Tropf, M.E. Thomas and T.J. Harris, Chapter 33: Properties of Crystals end Glasses, in Handbook of Optics: Devices Measurements and Properties, 2nd Edition, vol II, Michael Bass (Ed.) Mc. Graw-Hill, Inc. 1995.

28. J.H. Lee, A. Yoshikawa, T. Fukuda, Growth of MgO/$MgAl_2O_4$ eutectic crystals by the micro-pulling-down method and its characterization, J. Eur. Ceram Soc. 25 (2005) 1351.
29. B. M. Moshtaghioun, J. I. Peña, Non-Hall-Petch hardness dependence in ultrafine fibrous MgO-$MgAl_2O_4$ eutectic ceramics fabricated by the laser-heated floating zone (LFZ) method, J. Eur. Ceram Soc. 39 (2019) 3208.
30. F.L. Kennard, R.C. Bradt, V.S. Stubican, Eutectic solidification of MgO-$MgAl_2O_4$, J. Am. Ceram Soc. 56 (1973) 566.
31. F.L. Kennard, R.C. Bradt, V.S. Stubican, Mechanical properties of the directionally solidified MgO-$MgAl_2O_4$ eutectic, J. Am. Ceram Soc. 59 (1976) 160.
32. K. Orlinski, M. Romaniec, A. Malinowska, R. Diduszko, Growth-microstructure relationship in MgO-$MgAl_2O_4$ eutectic fabricated by mico-pulling down method with $MgAl_2O_4$ seed crystal, J. Eur. Ceram Soc. 39 (2019) 3843.
33. C. Rode, T. Bunch-Nielsen, K.K. Hansen, B. Grelk, Moisture damage with magnesium oxide boards in Danish façade structures, Energy. Proc. 132 (2017) 765.
34. A.M. Alper, R. N. Mcnally, P. H. Ribbe, R. C. Doman, The system MgO-$MgAl_2O_4$, J. Am. Ceram Soc. 45 (1968) 263.
35. C. F. Bohren, D. R. Huffman, Absorption and scattering of light by small particles, Wiley VCH Verlag GmbH and Co. KGaA, Weinheim (2004).
36. https://omlc.org/calc/mie_calc.html
37. RefractiveIndex.INFO website (https://refractiveindex.info/)
38. W. J. Tropf, M.E. Thomas, Magnesium aluminum spinel (MgAl2O4), in E.D. Palik (ed.), handbook of Optical Constants of Solids II, Academic Press, Orlando (1991) 881.
39. R.E. Stephens, I. H. Malitson, Index of refraction of magnesium Oxide, J. Res. Natl. Bur.

Stand. 49 (1952) 249.

40. K. Morita, B.K. Kim, K. Hiraga and H Yoshida, Fabrication of high strength transparent $MgAl_2O_4$- spinel polyscristals by optimizing spark-plasma-sintering conditions, J. Mat .Res. 24 (2009) 2863.

Submitted to Journal of the European Ceramics Society on 23th July 2019/ Revised 18th Oct/ Accepted 29th Oct.

## Figures

**Figure 1.**Representative FE-SEM micrographs (transverse sections) of $MgAl_2O_4$-MgO eutectic crystal grown by LFZ at (A) 10, (B) 25, (C) 50, (D) 100 and (E) 750 mm/h. For all images, the inset shows higher magnification to see MgO morphology.

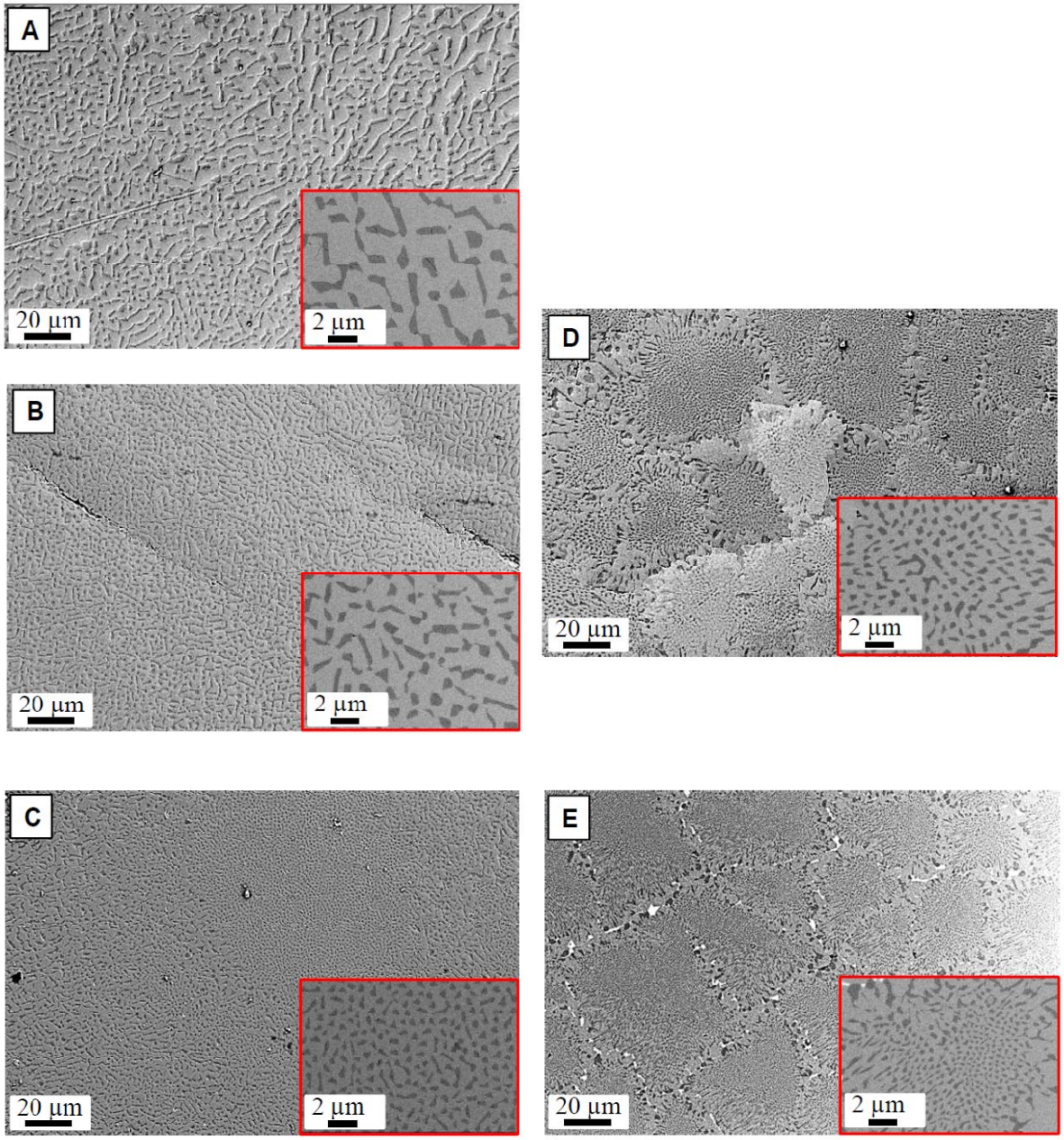

**Figure 2.**Measured transmission (in-line) of transverse slices of the DSE MgO-$MgAl_2O_4$ solidified without rotation. The slices used for the measurements were approximately 1 mm thick, and the shown spectra have been adjusted to this thickness for easy of comparison. Different colors correspond to different pulling rates (also indicated in the plot): black (10 mm/h), red (25 mm/h), orange (50 mm/h), blue (100 mm/h), magenta (750 mm/h). Orange dotted line: 50 mm/h measured with smaller diaphragm on a better aligned rod so that light travels along the solidification direction.

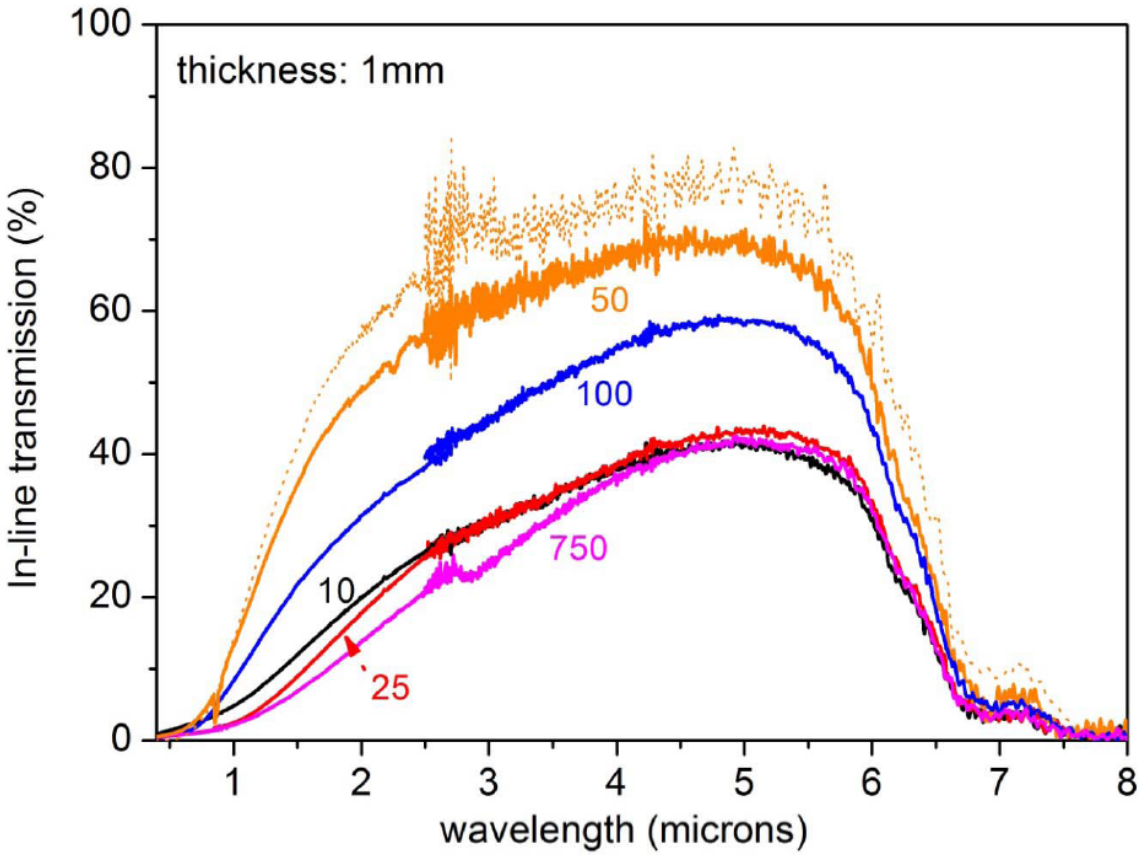

**Figure 3.**Measured transmission (in-line) of transverse slices of the DSE MgO-$MgAl_2O_4$ solidified with rotation. The microstructure of the samples showed some banding. The slices used for the measurements were approximately 1 mm thick, and the shown spectra have been rescaled to this thickness for easy of comparison. Different colors correspond to different pulling rates: black (50 mm/h), red (100 mm/h). Continuous lines correspond to transverse slices, dotted lines correspond to longitudinal slices. The absorption peak at around 5.8 μm in one of the measurements is due to epoxy-resin used for mounting.

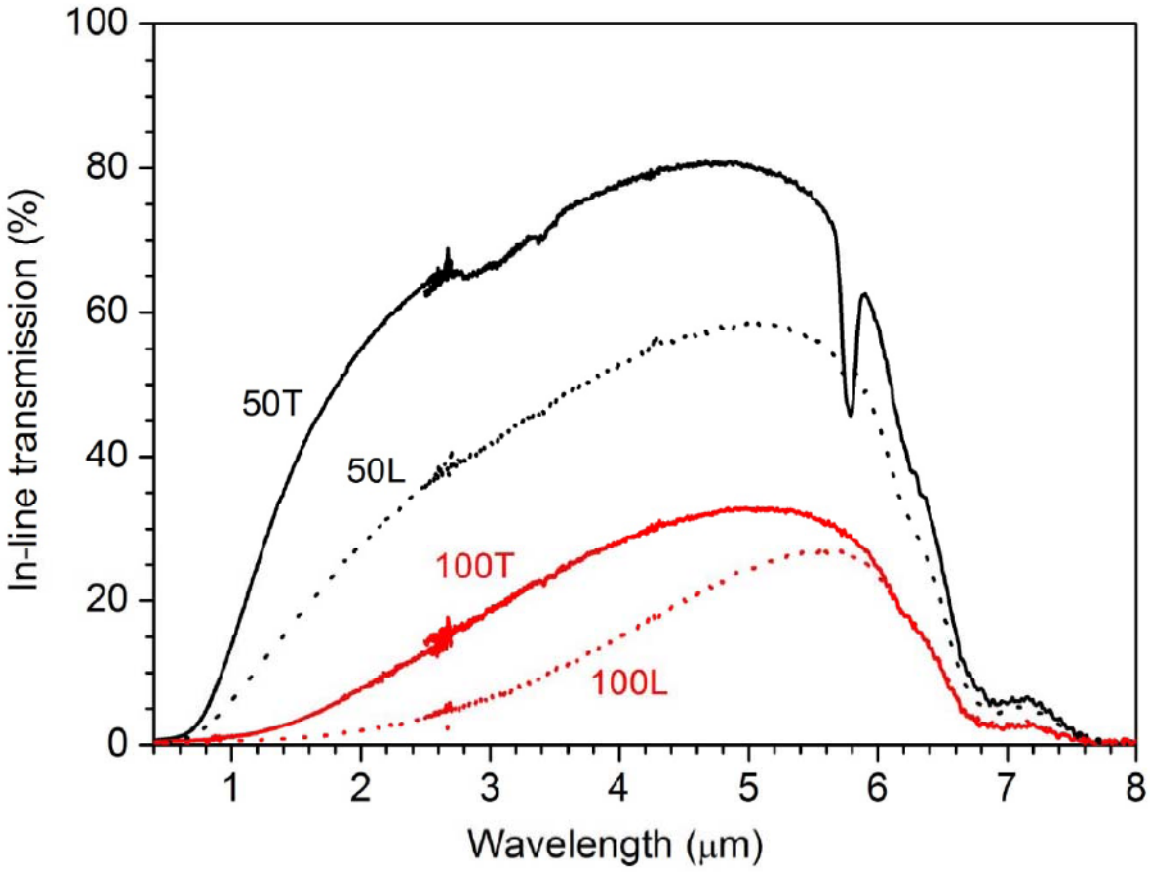

**Figure 4.**Simulated transmission (in-line) spectra calculated from Mie-scattering of non-interacting spheres of MgO (0.245 vol %) on $MgAl_2O_4$ matrix with different sphere diameters. Black squares (4.3 μm), red circles (3.2 μm), orange up-triangles (0.8 μm), brown down-triangles (1.9 μm), blue diamonds (0.9 μm (32%), 7.1 μm (32%) and 2.25 μm (36%)), magenta stars (0.34 μm (50%) and 2.08 μm (50%)).

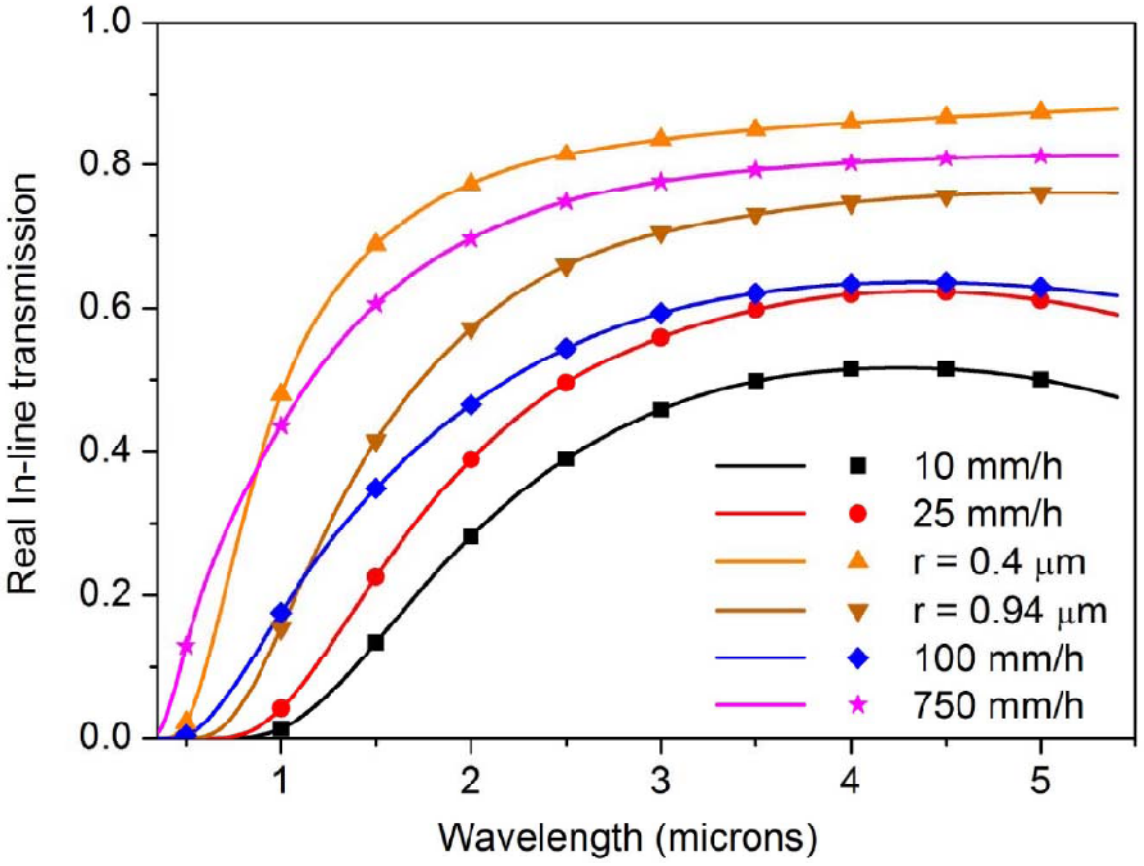

**Table 1.**Average transverse particle size used to describe the transverse size of the MgO dispersed phase in the samples grown at various rates by LFZ method. The transverse size has been determined from equivalent rod diameter in equiaxial MgO sections (rod microstructures or cell boundaries); or from <width+length>/2 in rod-to-lamellae microstructures.

| Sample | Pulling Rate (mm/h) | Transverse size MgO (μm) (and volume of sample assumed when applicable) | | | Comments |
|---|---|---|---|---|---|
| M10 | 10 mm/h | 4.3 μm | | | Rod-to-lamellae microstructure |
| M11 | 25 mm/h | 3.2 μm | | | Rod-to-lamellae microstructure |
| M12, M16 | 50 mm/h | 1.9 μm<br>In rod-to-lamellae regions | 0.8 μm<br>In rod microstructures at the center of the bar | | Rod (triangular section) and Rod-to-lamellae microstructure |
| M14 | 100 mm/h | 0.9 μm (32 % vol)<br>Core: inside cells. | 7.1 μm (32 % vol)<br>Core: cell boundaries. | 2.25 μm (36 % vol)<br>Outer shell. | Cells at the center, fibrous to interpenetrated at the outer shell |
| M15 | 750 mm/h | 0.34 μm (50 % vol)<br>Inside cells | 2.1 μm (50% vol)<br>Cell boundaries | | Cells all across the solidified sample.<br>Abundant micro-cracks at cell boundaries. Possible third phases. |